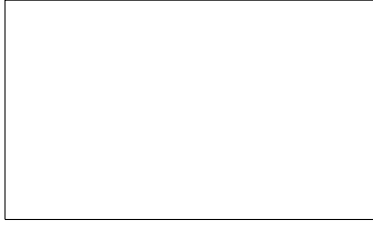


## Graphical Abstract

**Can we accurately calculate viscosity in multicomponent metallic melts?**

Nikolay Kondratyuk, Roman Ryltsev, Vladimir Ankudinov, Nikolay Chtchelkatchev



arXiv:2211.03483v1 [cond-mat.mtrl-sci] 7 Nov 2022

## Highlights

### **Can we accurately calculate viscosity in multicomponent metallic melts?**

Nikolay Kondratyuk, Roman Ryltsev, Vladimir Ankudinov, Nikolay Chtchelkatchev

- Deep machine learning potential is applied for simulating viscosity of Al-Cu-Ni melts
- Results match experimental viscosity dependencies on temperature and concentration
- Simulations reproduce the minimum of the viscosity at the eutectic composition
- Deep machine learning potentials predict viscosity of multicomponent metallic melts

# Can we accurately calculate viscosity in multicomponent metallic melts?

Nikolay Kondratyuk<sup>a,b,c</sup>, Roman Ryltsev<sup>d,e,f</sup>, Vladimir Ankudinov<sup>d</sup>, Nikolay Chtchelkatchev<sup>d</sup>

<sup>a</sup>*Moscow Institute of Physics and Technology (National Research University), Institutskiy Pereulok 9, Dolgoprudny, 141701, Moscow oblast, Russia*

<sup>b</sup>*Joint Institute for High Temperatures, Russian Academy of Sciences, Izhorskaya 13 Bldg 2, Moscow, 125412, Russia*

<sup>c</sup>*Higher School of Economics (National Research University), Myasnitskaya 20, Moscow, 101000, Russia*

<sup>d</sup>*Vereshchagin Institute of High Pressure Physics, Russian Academy of Sciences, Kaluzhskoe sh. 14, Moscow (Troitsk), 108840, Russia*

<sup>e</sup>*Institute of Metallurgy of the Ural Branch of the Russian Academy of Sciences, Amundsen str. 106, Ekaterinburg, 620016, Russia*

<sup>f</sup>*Ural Federal University, Lenin Ave, 51, Ekaterinburg, 620002, Russia*

---

## Abstract

Calculating viscosity in multicomponent metallic melts is a challenging task for both classical and *ab initio* molecular dynamics simulations methods. The former may not provide enough accuracy and the latter is too resource demanding. Machine learning potentials provide optimal balance between accuracy and computational efficiency and so seem very promising to solve this problem. Here we address simulating kinematic viscosity in ternary Al-Cu-Ni melts with using deep neural network potentials (DP) as implemented in the DeePMD-kit. We calculate both concentration and temperature dependencies of kinematic viscosity in Al-Cu-Ni and conclude that the developed potential allows one to simulate viscosity with high accuracy; the deviation from experimental data does not exceed 9% and is close to the uncertainty interval of experimental data. More importantly, our simulations reproduce minimum on concentration dependency of the viscosity at the eutectic point. Thus, we conclude that DP-based MD simulations is highly promising way to calculate viscosity in multicomponent metallic melts.

*Keywords:* viscosity, molecular dynamics, machine learning potentials, metallic melts

---

## 1. INTRODUCTION

An accurate calculation of transport coefficients in liquids, such as shear viscosity and diffusivity, is one of the most important tasks in condensed matter theory. Indeed, the characteristics of atomic transport are crucial for studying such fundamental processes as glass formation and nucleation as well as for constructing and verifying model theories of liquid state [1] and coarse grained phase-field models [2, 3, 4, 5]. From a practical point of view, the values of the transport coefficients of melts influence the performance of metallurgical casting and other pyrometallurgical processes, the creation of heat transfer fluids, the improvement of ion batteries, and the development of new lubricants, etc. [6].

A reliable experimental determination of the viscosity and the diffusivity is a difficult and sometimes nearly impossible task. Among common experimental difficulties are (i) high temperatures and pressures that can be hardly possible to achieve in the experiment (e.g. in silicate melts) [7]; (ii) strong chemical interaction of the melts with the environment and sample containers (e.g. for Al-based and Zr-based melts); (iii) low accuracy and/or high cost of certain experimental techniques (e.g., measuring of the diffusion coefficients) [8, 9]. In this regard, atomistic

computer simulations acquire a special role due to the possibility to calculate any characteristics of atomic transport based on the trajectories of particles. Within the molecular dynamics methods, the shear viscosity coefficients could be obtained via the equilibrium (Green-Kubo [10, 11], Helfand [12], finite size effects of diffusion [13, 14]) or non-equilibrium methods (Müller-Plathe [15], SLLOD [16]). At the same time, the methods for viscosity calculation are shown to be quite accurate for various systems from atomic [17, 18, 19, 20, 21, 22, 23] to molecular fluids [24, 25, 26, 27, 28, 29, 30]. In theory, the predictive power of such models depends only on the accuracy of the predefined interatomic forces. These forces could be described via the model potentials, Machine Learning Interatomic Potentials (MLIP) and Density-Functional Theory (DFT), which are listed in ascending order of the required computational resources. The key factor of the choice among this approaches is the balance between accuracy and computational efficiency [31, 32, 33].

Traditional methods based on classical molecular dynamics (CMD) operate with relatively simple model potentials and allow one to simulate systems of  $10^6 - 10^9$  atoms at times up to microseconds. These spatio-temporal scales are sufficient to obtain the shear viscosity coefficients via both equilibrium and non-equilibrium methods. For example, CMD with effective pair potentials resulted to the viscosity of liquid Li, Na and Rb in close agreement with

---

\*Corresponding address: kondratyuk@phystech.edu

experimental data [34, 35, 36]. The embedded atom model (EAM) [37, 38] is a wide spread multibody potential for the CMD simulations of metals. For liquid Na and Al, EAM potentials provide a relatively good accuracy for the calculated viscosity in comparison to the experiment [39, 40, 23]. On the other hand, the results for viscosity of Li [39] and Ni [41] melts obtained from EAM-based MD simulations deviate from experimental values by a factor of two. The review [42] shows that different functional forms of liquid Ni potential lead to the significantly differing values of viscosity. Moreover Mendeleev et al. [43] demonstrate that the potentials, which are parameterized for the properties of the crystalline phase only, poorly describe the liquid phase.

Thus, the accuracy of CMD is very much limited by using of the empirical potentials, which in many cases are unable to adequately approximate the complex nature of interatomic interactions in real systems. This is especially evident in the case of multicomponent metallic melts.

Meanwhile, highly accurate *ab initio* methods are very resource-demanding and therefore allow simulating physical systems only at spatio-temporal scales, which are insufficient for reliable calculation of viscosity. The crucial problem is the requirement of the relatively long trajectories to perform time averaging for the viscosity, since it is a collective property. These time scales are still very computationally expensive and hardly achievable by DFT. A possible solution is to use indirect diffusivity-based methods like the Stokes-Einstein (S-E) relation where the diffusivity multiplied by the viscosity is proportional to the temperature of the system and the inverse hydrodynamic radius of a particle. The methods for calculation of the diffusion constants use the ensemble averaging in addition to the time averaging, and therefore are achievable within DFT method. This method of the shear viscosity estimations was applied to  $\text{Al}_{80}\text{Cu}_{20}$  [44],  $\text{GeTe}$  [45], and  $\text{NaCl-CaCl}_2$  [46]. Adjaoud et al. [47] show the applicability of the S-E relation for liquid  $\text{Mg}_2\text{SiO}_4$  in a wide range of pressures and temperatures. However, the problem with the S-E method arises when considering multi-component systems: the diffusivity becomes a tensor and it stays unclear which component of the tensor should be used for the estimations.

Thus, we conclude that accurate calculation of the shear viscosity in multicomponent metallic melts is a challenging task because it requires both high accuracy and high computational efficiency. Fortunately, a machine-learning-based approach has recently emerged that makes it possible to effectively solve this problem [48, 49, 50, 51, 52, 53, 54, 55]. The idea is to approximate the potential energy surface of the system by some general many-body function (for example, a multilayer neural network) using reference *ab initio* data. Such machine learning interatomic potentials (MLIPs) can provide a nearly *ab initio* accuracy with several orders of magnitude less computational costs [56]. In comparison with traditional analytical MD potentials, usage of MLIPs is especially beneficial for the systems with highly diverse local atomic environment: e.g.

for high-entropy metal alloys [57] or for multiphase carbon systems [58, 59].

Despite high potential of using MLIPs to calculate viscosity in metallic melts, there are only few examples of such application in published literature for the best of our knowledge. Lopanitsyna et al. [60] developed such a potential for liquid Ni and obtain the temperature dependence of the viscosity via finite size effects of diffusion. A reasonable agreement with experimental data was achieved. Another example, is a successive use of deep machine learning potential for calculating viscosity of liquid gallium [61]. The mentioned papers address viscosity of pure metals; as far as we know, similar works devoted to even binary metallic melts are absent. The authors familiar with only a recent successful application of MLIPs for the viscosity of molten binary salts [62]. The possible reasons are the relative novelty of MLIP-based simulations and the lack of reliable experimental data on the viscosity of multi-component melts.

Here we make a step to fill this gap and apply MLIP-based simulations for calculating shear viscosity in the ternary Al-Cu-Ni system. This system demonstrates complicated chemical interaction between its components, which leads to a non-monotonous behaviour of the kinematic viscosity as a function of a concentration [63].

## 2. Neural network potential

### 2.1. Training procedure

As a tool for developing MLIPs, we use DeePMD-kit, which utilizes feedforward multilayer neural networks to build highly accurate and efficient interatomic potentials (hereafter, Deep Potentials (DP)) [64]. Among other similar approaches, DeePMD uses an effective and automatic procedure for mapping the particles' coordinates to the space of structural descriptors, which includes many-body interactions and provides invariance with respect to translations, rotations, and permutations. Another advantage is the DPGEN tool, which utilizes concurrent learning strategy [65, 66] for generating compact and representative training datasets and creating DPs, which are uniformly accurate in the whole space of thermodynamic parameters. This approach has been successfully applied for simulating systems of different nature [64, 67, 68, 69, 70, 71, 72, 73, 74, 75].

The training dataset for DP's developing was generated within the framework of concurrent learning strategy using DPGEN package by the following scheme. We considered 14 compositions along the  $\text{Al}_{100-x}\text{Cu}_x\text{Ni}_{10}$  cross-section where  $x$  varied in range of 17 – 40 at.%. For each composition, we generate by *ab initio* molecular dynamics simulations a supercell of 512 atoms which structure corresponds to the equilibrium melt. These configurations has been applied as initial ones for concurrent learning procedure.

Concurrent learning as implemented in DeePMD and DPGEN packages is an iterative procedure, which consists

Table 1: Details of networks structure and training scheme used to generate DPs. The vectors determining the structure of both embedding and fitting nets contain the numbers of the neurons in each network layer. The cutoffs vector is  $(r_{cs}, r_c)$ , where  $r_{cs}$  is the smooth cutoff parameter and  $r_c$  is the cutoff radius of the model. The learning scheme vectors contain the start and end values of loss function contributions from energies, forces and virial tensors, respectively.

embedding net	axis neuron	fitting net	cutoffs	learning scheme
(25, 50, 100)	8	(240, 240, 240)	(1.5,7)	(0.1, 1.0); (1000, 1.0); (0.05, 0.1)

of three repeating stages. At the first (training) stage, we use the dataset to train an ensemble of four DPs with different initializations of neural network weights. As the initial dataset we used several tens of configurations and corresponding values of energies, forces and virial tensors extracted from *ab initio* molecular dynamics simulations. The parameters used for the training are presented in Tab. 1. Each model was trained for 400,000 iterations with the batch size equal to 1.

At the second (exploration) stage, we use one of the DPs obtained from the ensemble to perform CMD simulations of 14  $\text{Al}_{100-x}\text{Cu}_x\text{Ni}_{10}$  alloys at temperature  $T = 1600$  K, which corresponds to equilibrium liquid for all compositions under consideration. The length of each MD run was 25 ps (25,000 steps of 1 fs). At each MD step, we perform analysis of resulting atomic configurations and select candidates for DFT labelling and including to an extended training dataset. The selection criterion is the value of the model deviation parameter  $\epsilon$ , which is the maximal deviation of the forces predicted by the ensemble of models. The idea behind this parameter is very simple. For 'good' configurations, which are reliably described by a DP,  $\epsilon$  is expected to be small. If  $\epsilon$  is rather large, then corresponding configuration probably belongs to the extrapolation region for current dataset (not covered by the training data) and thus should be treated as a candidate for DFT labelling. In practice, one should determine two parameters: upper  $\sigma_{up}$ , and lower  $\sigma_{lo}$  trust levels, which are used to select configurations for labelling. The configuration is selected if only  $\sigma_{lo} \leq \epsilon \leq \sigma_{up}$ . In our study we use  $\sigma_{lo} = 0.05$ ,  $\sigma_{up} = 0.15$ . After selecting all candidate structures, a fixed number (100 in our case) of them with the highest values of  $\epsilon$  are used for labelling.

During the next (labelling) stage, for each atomic configuration selected during the exploration stage, reference values of energy, forces and virial tensors are calculated by density functional theory (DFT) as implemented in Vienna *ab initio* simulation program (VASP) [76]. Projector augmented-wave (PAW) pseudopotentials and Perdew-Burke-Ernzerhof (PBE) [77, 78] gradient approximation to the exchange-correlation functional [79] were applied. To sample the Brillouin zone only the  $\Gamma$  point was used. Energy cutoff and other related parameters was set in accordance to built-in precision parameter  $\text{PREC}=\text{Normal}$ .

The described above stages was repeated until the selection procedure is saturated that means the inequality  $\epsilon \leq \sigma_{lo}$  is satisfied for all the configurations generated at the exploration stage. The resulting dataset in-

cludes about 10,000 atomic configurations and corresponding values of energies, forces and virial tensors calculated by DFT.

## 2.2. Verification of DP

Before calculating the viscosity, we verify the predictability of the developed DP in comparison to *ab initio* data. A standard first test is to check how the potential reproduces DFT values of energies, forces and virial tensors. In Fig. 1 we show DP vs DFT correlations for these quantities calculated on a validation dataset including data from all compositions. One can find a pronounced linear correlation between presented data. The values of RMSEs for energy, forces, and virials are respectively 1.4 meV/atom, 81 meV/Å and 7.96 meV/atom. So we expect that the potential would provide a good accuracy in simulations of the observable properties of Al-Cu-Ni melts at least for  $\text{Al}_{100-x}\text{Cu}_x\text{Ni}_{10}$  compositions. To check this point, we have extracted partial radial distribution functions (RDFs) and velocity autocorrelation functions (VAFs) of the melts from both *ab initio* molecular dynamics (AIMD) and DP simulations and obtained close agreement between these data. In Fig. 2 we illustrate this result with the example of  $\text{Al}_{72.5}\text{Cu}_{17.5}\text{Ni}_{10}$  melt at  $T = 1673$  K. Thus, we conclude that developed potential reproduce structural and dynamic properties of Al-Cu-Ni melts with *ab initio* accuracy.

## 3. Viscosity calculations

The shear viscosity  $\eta$  of melt can be obtained using both equilibrium (Green-Kubo) (G-K) and reverse non-equilibrium (Müller-Plathe) (M-P) methods, here we use them for the verification of each other. The kinematic viscosity  $\nu$  is obtained as  $\eta/\rho$ , where  $\rho$  is the equilibrium density at a given temperature  $T$ .

### 3.1. Non-equilibrium method

The viscosity of liquids and fluids can be calculated by the reverse non-equilibrium molecular dynamics (RNEMD) approach [80]. It imposes momentum transfer in the simulation cell. As a response, a velocity gradient is established. The ratio of the momentum flux to the velocity gradient gives the shear viscosity:

$$\eta = \frac{j_z(p_x)}{\partial v_x / \partial z} \quad (1)$$

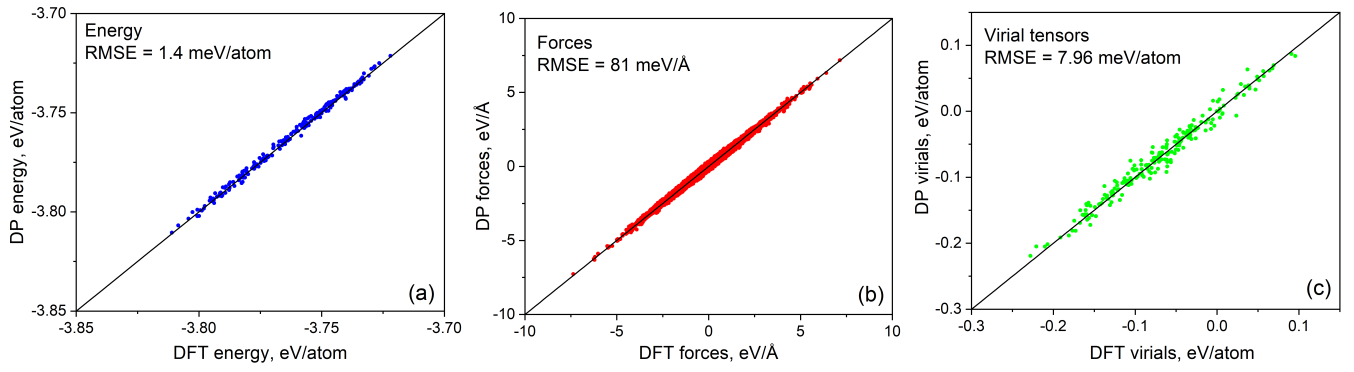


Figure 1: DP-based MD simulation results vs obtained using DFT for: (a) energies, (b) forces and (c) virial tensors for Al-Cu-Ni melts.

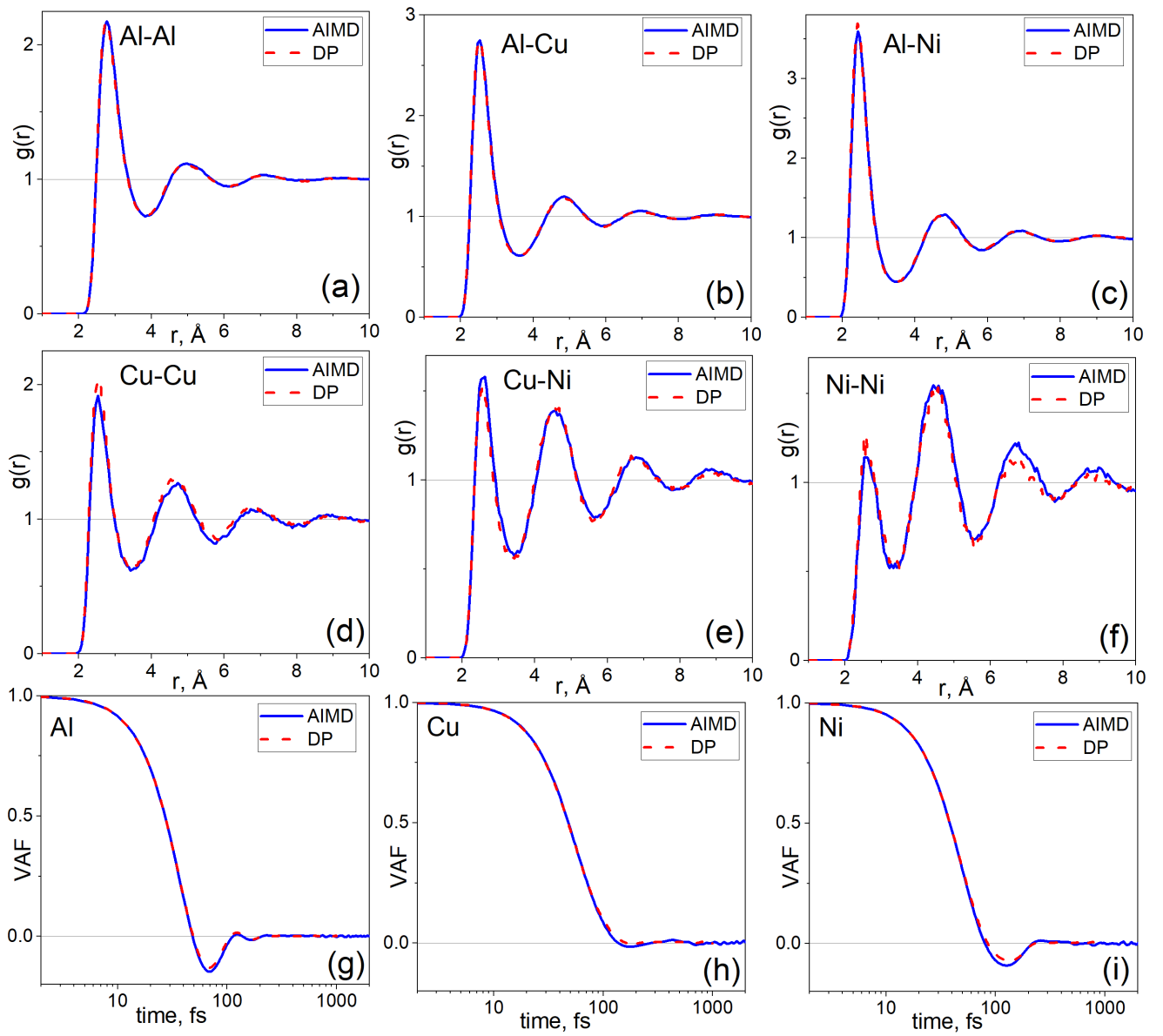


Figure 2: Partial radial distribution functions (a-f) and velocity autocorrelation functions (g-i) for  $\text{Al}_{72.5}\text{Cu}_{17.5}\text{Ni}_{10}$  melt at  $T = 1673$  K extracted from AIMD simulations (solid blue lines) as well as from DP simulations (red dashed lines).

where  $j_z(p_x)$  is the flux of the  $x$ -component of momentum, and  $\partial v_x/\partial z$  is the  $x$ -component of velocity gradient, both of them in  $z$  direction.

To create the flow in the melts, we use `fix viscosity` command implemented in LAMMPS [81]. The cell is divided into 50 bins in  $Z$  direction, and the average velocity of the group of atoms in each layer is calculated. Then, the velocities of Al atoms in the bottom and middle bins at each N step are swapped. As a result of such a procedure, the Couette flow is established in the unit cell.

### 3.2. Equilibrium method

In our previous papers, we have shown that the non-equilibrium simulation results converge to the Green–Kubo (G–K) values as the strain rate or the corresponding momentum flux decreases [82, 83]. Thus, it is reasonable to use Green–Kubo technique because it gives zero shear rate values of viscosity.

The Green–Kubo formula for the shear viscosity  $\eta_{\alpha\beta}$  in  $\alpha\beta$ -plane is [10, 11]:

$$\eta_{\alpha\beta} = \lim_{t' \rightarrow \infty} \frac{V}{k_B T} \int_0^{t'} C_\sigma(t) dt, \quad (2)$$

$$C_\sigma(t) = \langle \sigma_{\alpha\beta}(0) \sigma_{\alpha\beta}(t) \rangle, \quad (3)$$

where  $C_\sigma(t)$  is a shear-stress autocorrelation function (SACF), which averaging over the canonical ensemble is denoted by  $\langle \dots \rangle$ ,  $\sigma_{\alpha\beta}$  are shear components of the stress tensor,  $V$  and  $T$  are respectively system volume and temperature, and  $k_B$  is the Boltzmann’s constant. In practice, the integral in Eq. (2) is typically calculated up to some finite time  $t'$  when  $C_\sigma$  decays to zero within the accuracy of numerical simulation. The shear viscosity  $\eta$  can be found as an average of  $\eta_{xy}$ ,  $\eta_{xz}$  and  $\eta_{yz}$ .

The stress tensor  $\sigma_{\alpha\beta}$  is calculated from the following equation:

$$\sigma_{\alpha\beta} V = \sum_{i=1}^N m_i v_{i\alpha} v_{i\beta} + \sum_{i=1}^{N'} r_{i\alpha} f_{i\beta}, \quad (4)$$

where  $N$  is a number of atoms,  $N'$  includes atoms from neighboring sub-domains,  $r_{i\alpha}$  and  $v_{i\alpha}$  are  $\alpha$ -components of coordinate and velocity of the  $i$ -th atom, and  $f_{i\alpha}$  is  $\alpha$ -component of the force that acts on the  $i$ -th atom.

For effective averaging of G–K integrals, we use the time decomposition method (TDM) proposed by Maginn and co-authors [84]. In this method, the G–K integral was averaged over a number of independent MD runs and then should be fitted by the double exponential function

$$\eta(t) = A \cdot \alpha \cdot \tau_1 \cdot (1 - e^{-t/\tau_1}) + A \cdot (1 - \alpha) \cdot \tau_2 \cdot (1 - e^{-t/\tau_2}), \quad (5)$$

where  $A$ ,  $\alpha$ ,  $\tau_1$  and  $\tau_2$  are the fitting parameters. The SACFs are calculated in LAMMPS during the simulations via the `fix ave/correlate` command.

### 3.3. MD Simulation details

Initial configurations for all  $\text{Al}_{100-x}\text{Cu}_x\text{Ni}_{10}$  compositions are taken from the corresponding DFT simulations on which the DP was built. These configurations consist of 512 atoms with different compositions of Al, Cu and Ni atoms. We create 2x2x2 supercells of these configurations and carry out density equilibrations for 50 ps in the isothermal-isobaric ensemble (NPT) using the Nosé–Hoover barostat/thermostat [85, 86, 87] with 1 fs integration timestep. After the NPT relaxation, we compress the unit cells to the average values of densities for 10 ps. The example of the unit cell for  $\text{Al}_{72.5}\text{Cu}_{17.5}\text{Ni}_{10}$  melt is shown in Fig. 3.

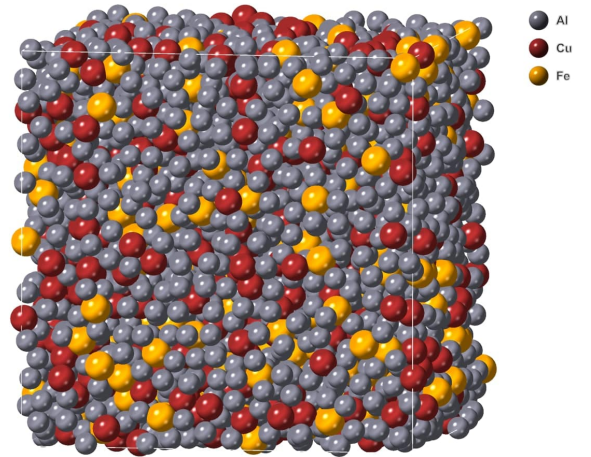


Figure 3: The snapshot of  $\text{Al}_{72.5}\text{Cu}_{17.5}\text{Ni}_{10}$  melt with 4096 particles in the cell (Al – silver, Cu – red, and Ni – golden) used in the DP simulations with DP potential in LAMMPS.

For the Green–Kubo calculations, we use about 100 trajectories of 50 ps length in the canonical ensemble to produce averaged SACFs. This length of a single trajectory is found to be enough for the statistical independence between each SACF, based on the diffusion coefficients of atoms. For RNEMD simulations, we carried out 1 ns-long trajectories to produce the velocity profiles. The first 50 ps were excluded from the consideration because of flow establishment.

## 4. Viscosity of Al–Cu–Ni melts

### 4.1. Verification of methods

To verify the kinematic viscosity calculation approach, we carry out both equilibrium Green–Kubo (G–K) and non-equilibrium Müller–Plathe (M–P) simulations for  $\text{Al}_{66}\text{Cu}_{24}\text{Ni}_{10}$  melt at 1673 K.

The dependence of G–K integral (2) on the upper time limit is shown in Fig. 4. Solid lines represent the results

for statistically independent MD trajectories. The average values of G–K integral at each upper time limit are shown with red points. One can find, while separate trajectories reveal large fluctuations of G–K integral, the average value converges to a well defined value at about 1 ps. We approximate the averaged values with the double exponential function Eq. (5) treating the points with the weight  $\sigma^{-1/2}$ , where  $\sigma$  is a standard deviation calculated over independent MD trajectories. The final value of kinematic viscosity  $\nu$  was found as the infinite time limit of the approximation Eq. (5) divided by the equilibrium density  $\rho$  at given temperature  $T = 1673$  K which is equal to  $3.741$  g/cm<sup>3</sup> for Al<sub>66</sub>Cu<sub>24</sub>Ni<sub>10</sub>. Thus, the resulting value is  $(3.9 \pm 0.2) \cdot 10^{-7}$  m<sup>2</sup>/s.

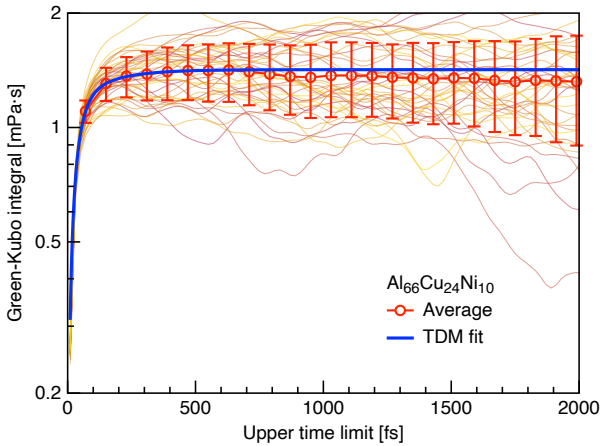


Figure 4: The dependence of Green–Kubo integral on the upper time limit for Al<sub>66</sub>Cu<sub>24</sub>Ni<sub>10</sub> melt at  $T=1673$  K,  $\rho = 3.741$  g/cm<sup>3</sup>.

Moreover we studied the kinematic viscosity dependence on the strain rate in the M–P method. For this purpose, the swapping frequency of Al atoms velocities in bottom and middle bins is varied, which establishes different values of strain rates (See Sec. 3.1 for details). The obtained velocity profiles are shown in Fig. 5a for different values of swap rates. The profiles are linear, which corresponds to Couette flow regime.

The dependence of the kinematic viscosity on the shear rate  $\dot{\gamma}$  is shown in Fig. 5b. One can see, for the considered shear rates the kinematic viscosity grows monotonically as the  $\dot{\gamma}$  decreases. Such non-Newtonian response is an expected behaviour for atomic [88] and molecular [82] liquids at the shear rates achievable in MD. For liquid copper, Han et al. [88] observed similar non-Newtonian dependence  $\eta(\dot{\gamma})$  via RNEMD and used the following approximation equation to calculate zero-shear viscosity  $\eta_0$ :

$$\eta = \eta_0 + A_1 \dot{\gamma}^{1/2}. \quad (6)$$

This equation is a consequence of Mode Coupling Theory [89]. We use the same equation to fit obtained  $\nu(\dot{\gamma})$  dependence for Al<sub>66</sub>Cu<sub>24</sub>Ni<sub>10</sub> melt. The resulting approximation curve is presented by solid blue line in 5b. Excellent agreement with the RNEMD results is achieved.

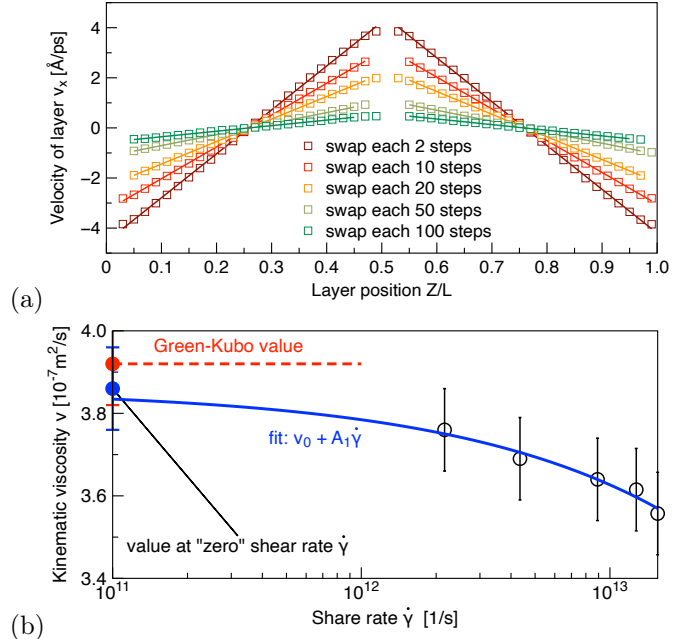


Figure 5: (a) The velocity profiles obtained via RNEMD simulation for Al<sub>66</sub>Cu<sub>24</sub>Ni<sub>10</sub> melt at  $T = 1673$  K,  $\rho = 3.741$  g/cm<sup>3</sup> for the different values of momentum fluxes. (b) The dependence of the kinematic viscosity on the shear rate. The red point shows the equilibrium value of viscosity calculated via the Green–Kubo method. The blue one is the value at  $\dot{\gamma} = 0$ , found from Eq.(6).

The value of zero shear rate kinematic viscosity from this approximation is  $(3.85 \pm 0.2) \cdot 10^{-7}$  m<sup>2</sup>/s.

It was suggested, that for ionic liquids, there are two regimes for  $\eta(\dot{\gamma})$  could appear, this caused as a consequence of different relaxation times of internal molecular degrees of freedom [90, 91]. As one can see from Fig. 5b, here only a single regime is observed that is rather expected from equilibrium metallic melts.

Thus, we conclude that the kinematic viscosity coefficients obtained by both equilibrium (G–K) and non-equilibrium (M–P) methods agree within the accuracy of the methods. That confirms that the predicting power of MD simulations of the viscosity is determined only by the developed potential. In the following, the Green–Kubo method is used to calculate the zero-shear kinematic viscosity in Al–Cu–Ni melts.

#### 4.2. Concentration dependence of the viscosity

A challenging task for any theoretical method is a calculation of the concentration dependencies of the viscosity in metallic melts. Such dependencies often demonstrate a non-monotonic behavior with extrema located in the vicinity of phase boundaries on phase diagrams [63, 92, 93, 94]. The unequivocal explanation of such behavior is not always available but it is obviously caused by a change in chemical interaction and local structure of melts during the concentration change. The simulation of such non-linear behaviour of the viscosity change is a complicated



problem and can be treated as a stress-test for machine learning potentials.

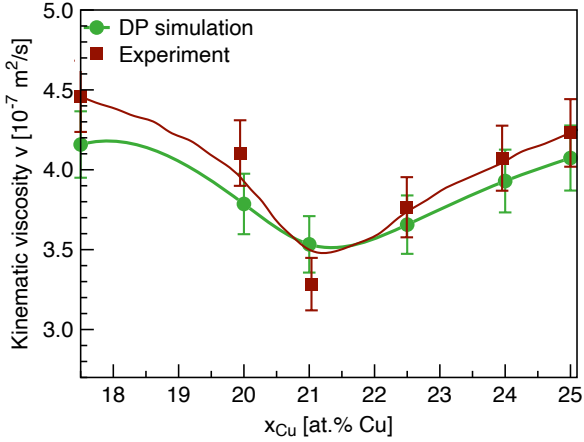


Figure 6: The kinematic shear viscosity  $\nu$  dependence on the  $x_{\text{Cu}}$  at.% concentration for  $\text{Al}_{100-x}\text{Cu}_x\text{Ni}_{10}$  melt at  $T=1673$  K. Green points are the results of the current work (with curve in order to guide the eye). Red points are the experimental data from [63] with the approximation curve.

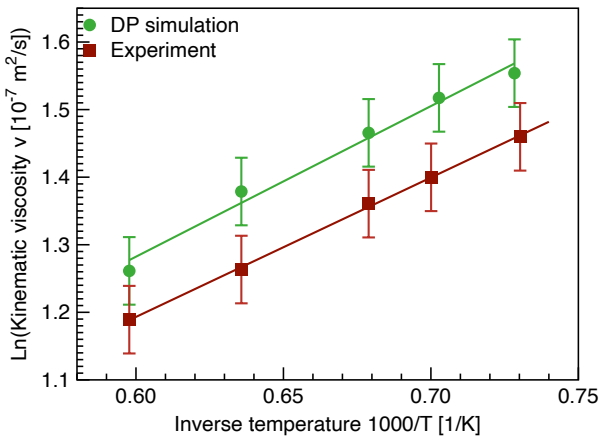


Figure 7: The dependence of log of kinematic shear viscosity  $\ln(\nu)$  for  $\text{Al}_{69}\text{Cu}_{21}\text{Ni}_{10}$  melt on the inverse temperature  $1000/T$ . Green and red bullets represent respectively simulated and experimental [63] data.

In 2017, Mudry et al. [95] studied the influence of Ni additions on viscosity of  $\text{Al}_2\text{Cu}$  melt. They demonstrated the viscosity decrease with the Ni addition due to the structural changes in the liquid. Recently, we experimentally observed that the kinematic viscosity in  $\text{Al}_{100-x}\text{Cu}_x\text{Ni}_{10}$  melts experiences a minimum at  $x_{\text{Cu}} = 21$  at.% which corresponds to the eutectic point [63]. To check whether this behaviour is reproduced by DP-based MD simulation, we calculated the kinematic viscosity coefficients along correspondent concentration cross-section at  $T = 1673$  K varying  $x_{\text{Cu}}$  in the range of 19-25 at.%. The comparison of experimental data from [63] and simulation results obtained

in present work are presented in Fig. 6. One can see that DP-simulations provide the quantitative agreement with experimental data; the simulated  $\nu(x)$  curve reproduces the minimum at eutectic point; the average deviation from experiment is about 8 % and the maximum deviation is 9 %. Such results should be considered as very accurate, taking into account the complexity of the problem.

#### 4.3. Temperature dependence of the viscosity

To test whether the developed potential reproduces the temperature dependence of viscosity, we carry out the G-K calculations for  $\text{Al}_{69}\text{Cu}_{21}\text{Ni}_{10}$  melt at different temperatures. The temperature range was 1373–1673 K, in which the system remains liquid according to both experimental results and our simulations. Before the viscosity calculations, NPT relaxations for 50 ps are carried out to determine equilibrium densities. Then, we deform the unit cells to the corresponding target densities. The comparison of the calculated temperature dependency of kinematic viscosity with the experimental data is presented in Fig. 7. One can see that  $\ln \nu$  vs  $1/T$  curves for experimental and simulated data are the linear slopes and both have very close slope angles. Thus, the Arrhenius equation can be used to approximate the obtained polytherms, which assumes the momentum transport as an activated rate process with activation energy  $E_a$ :

$$\nu = \nu_0 \exp(E_a/k_B T), \quad (7)$$

where  $\nu_0$  is a pre-exponential constant under investigation. It is widely accepted that Arrhenius equation is a good approximation for many metals and metallic alloys [96, 97, 98].

The Arrhenius fit gives  $\nu_0=9.57 \cdot 10^{-8}$  m<sup>2</sup>/s,  $E_a = 17.15$  kJ/mol for the experimental data and  $\nu_0=9.47 \cdot 10^{-8}$  m<sup>2</sup>/s,  $E_a = 18.53$  kJ/mol for our simulations data. Thus, the developed DP almost reproduces the pre-factor  $\nu_0$  and slightly underestimates the activation barrier  $E_a$ .

## 5. DISCUSSION AND CONCLUSIONS

In the present paper we address the question of if one can accurately calculate the viscosity in multicomponent metallic melts. As we mentioned above, neither traditional classical molecular dynamics (MD) (based on empirical potentials like embedded-atom method [EAM] potentials) nor *ab initio* can not be considered as an effective and universal tool for solving this problem. The former approach usually suffers from lack of accuracy and the latter is too time-consuming and so usually cannot provide enough statistics. A possible solution is the use of machine learning potentials which demonstrate optimal accuracy/efficiency ratio. Here we make a first step to check this idea.

Considering deep neural network potentials (DP) as a regression model for machine learning potentials and DeePMD-kit as a powerful tool for their development, we

calculate both concentration and temperature dependencies of kinematic viscosity in Al-Cu-Ni melts. The main results are presented in Figs. 6, 7. Analysing the results, we conclude that the developed DP allows one to calculate viscosity with high accuracy; the deviation from experimental data does not exceed 9% and is close to the uncertainty interval of experimental data. More importantly, DP-based MD simulations reproduce the minimum on concentration dependency of the viscosity at the eutectic point. Thus, we response that for the Al-Cu-Ni melts one can positively answer to the main question raised in the title of the paper.

Despite the general success in calculating of the viscosity of Al-Cu-Ni melts, the agreement between theory and experiment is not perfect. Now we discuss briefly the possible reasons for such deviation from experimental data and general ways to improve the results.

First, it should be noted that measurement of the viscosity of metallic melts is a complicated experimental procedure especially in the case of alloys with high liquidus temperatures ( $> 1000$  K) [99, 100]. As a result, experimental data obtained for the same system by different methods and/or on different devices can differ from each other by several times (see, for example, [101, 102] for Al and its alloys). We use experimental data obtained with an oscillating vessel viscometer using precise and carefully approved procedure [103]. However, some systematic errors caused by the individual characteristics of the experimental device are possible here. Unfortunately, for the best of our knowledge, we do not know the alternative data for the viscosity of Al-Cu-Ni melts and so can not fully get rid of this error.

Besides experimental difficulties discussed above, there are many sources of uncertainties in calculating shear viscosity via MD simulations. The main ones are: (i) statistical errors, (ii) finite-size effects, and (iii) imperfections of interatomic potentials. Recently, Kim et al. [20] carefully analyzed the first two of them. Based on their findings and taking into account the results of the method verification presented above, we can declare that our calculations are not noticeably affected by the finite size effects and by the lack of statistics. Thus, the main source of uncertainties in our simulations can come from possible drawbacks of the potential.

Again, there are many reasons that can cause inaccuracies in machine learning interatomic potentials, such as insufficient training dataset, poor functional form of the potential and errors in training procedure. We carefully verify our DPs and conclude that it provides *ab initio* accuracy for interatomic energies, forces and virial tensors. Thus, the only noticeable source of DP imperfection is an inaccuracy in *ab initio* data itself. This inaccuracy may be noticeable when one applies standard DFT calculations for transition metals (see, for example, our recent results for pure Ni [67]). We suppose that this problem can be even more serious when considering melts containing four and more elements including transition metals. A possible so-

lution in this situation is going beyond DFT to generate training dataset. This is an urgent challenging task, whose applicability extends well beyond the problem of viscosity calculation.

Anyway, here we declare that the accuracy achieved in this paper for ternary metallic melt is high enough and so ML-based MD simulations is highly promising way to calculate viscosity in multicomponent metallic melts. Moreover in this perspective, dare we hope not only for reproduction of the experimental results but that one can apply the described procedure on the prediction of the melts properties.

## ACKNOWLEDGEMENTS

We thank L. Kamaeva for helpful discussions of experimental data and techniques. This work was supported by the Russian Science Foundation (grant 22-22-00506). N. Kondratyuk was supported by the strategic academic leadership program ‘‘Priority 2030’’ (Agreement 075-02-2021-1316 30.09.2021). The numerical calculations are carried out using computing resources of the federal collective usage center ‘Complex for Simulation and Data Processing for Mega-science Facilities’ at NRC ‘Kurchatov Institute’ (ckp.nrcki.ru), supercomputers at Joint Supercomputer Center of Russian Academy of Sciences (www.jsc.c.ru), ‘Uran’ supercomputer of IMM UB RAS (parallel.uran.ru) and HPC facilities at HSE University [104].

## Data Availability Statement

The data that supports the findings of this study is available from N.K. upon reasonable request.

## References

- [1] A. J. Archer, Dynamical density functional theory for dense atomic liquids, *Journal of Physics Condensed Matter* 18 (24) (2006) 5617–5628. doi:10.1088/0953-8984/18/24/004.
- [2] P. F. Tupper, M. Grant, Phase field crystals as a coarse-graining in time of molecular dynamics, *EPL* 81 (4) (2008) 40007. doi:10.1209/0295-5075/81/40007.
- [3] Q. Bronchart, Y. Le Bouar, A. Finel, New coarse-grained derivation of a phase field model for precipitation, *Physical Review Letters* 100 (1) (2008) 015702. doi:10.1103/PhysRevLett.100.015702.
- [4] D. Jou, P. K. Galenko, Coarse graining for the phase-field model of fast phase transitions, *Phys Rev E* 88 (4) (2013) 042151. doi:10.1103/PhysRevE.88.042151.
- [5] V. Ankudinov, K. R. Elder, P. K. Galenko, Traveling waves of the solidification and melting of cubic crystal lattices, *Physical Review E* 102 (6) (2020) 062802. doi:10.1103/PhysRevE.102.062802.
- [6] C. Meier, R. W. Penny, Y. Zou, J. S. Gibbs, A. J. Hart, *Thermophysical Phenomena in Metal Additive Manufacturing By Selective Laser Melting: Fundamentals, Modeling, Simulation, and Experimentation*, *Annual Review of Heat Transfer* 20 (1) (2018) 241–316. doi:10.1615/annualrevheattransfer.2018019042.
- [7] H. Ni, H. Hui, G. Steinle-Neumann, Transport properties of silicate melts, *Reviews of Geophysics* 53 (3) (2015) 715–744. doi:10.1002/2015RG000485.

- [8] T. Masaki, T. Fukazawa, S. Matsumoto, T. Itami, S. Yoda, Measurements of diffusion coefficients of metallic melt under microgravity—current status of the development of shear cell technique towards JEM on ISS, *Measurement Science and Technology* 16 (2) (2005) 327–335. doi:10.1088/0957-0233/16/2/002.
- [9] A. Meyer, The measurement of self-diffusion coefficients in liquid metals with quasielastic neutron scattering, *EPJ Web of Conferences* 83 (2015) 01002. doi:10.1051/epjconf/20158301002.
- [10] M. S. Green, Markoff Random Processes and the Statistical Mechanics of Time-Dependent Phenomena. II. Irreversible Processes in Fluids, *J. Chem. Phys.* 22 (3) (1954) 398. doi:10.1063/1.1740082.
- [11] R. Kubo, Statistical-Mechanical Theory of Irreversible Processes. I. General Theory and Simple Applications to Magnetic and Conduction Problems, *J. Phys. Soc. Jpn.* 12 (6) (1957) 570–586. doi:10.1143/JPSJ.12.570.
- [12] E. Helfand, Transport Coefficients from Dissipation in a Canonical Ensemble, *Physical Review* 119 (1) (1960) 1–9. doi:10.1103/PhysRev.119.1.
- [13] S. H. Jamali, L. Wolff, T. M. Becker, A. Bardow, T. J. H. Vlugt, O. A. Moulton, Finite-Size Effects of Binary Mutual Diffusion Coefficients from Molecular Dynamics, *Journal of Chemical Theory and Computation* 14 (5) (2018) 2667–2677. doi:10.1021/acs.jctc.8b00170.
- [14] M. Orekhov, Improving molecular dynamics calculation of diffusivity in liquids with theoretical models, *Journal of Molecular Liquids* 322 (2021) 114554. doi:10.1016/j.molliq.2020.114554.
- [15] P. Bordat, F. Müller-Plathe, The shear viscosity of molecular fluids: A calculation by reverse nonequilibrium molecular dynamics, *The Journal of Chemical Physics* 116 (8) (2002) 3362–3369. doi:10.1063/1.1436124.
- [16] C. J. Mundy, J. I. Siepmann, M. L. Klein, Decane under shear: A molecular dynamics study using reversible nvt-sllod and npt-sllod algorithms, *The Journal of Chemical Physics* 103 (23) (1995) 10192–10200. doi:10.1063/1.469922.
- [17] A. Y. Kuksin, G. Norman, V. Pisarev, V. Stegailov, A. Yanilkin, Theory and molecular dynamics modeling of spall fracture in liquids, *Physical Review B* 82 (17) (2010) 174101.
- [18] r. D. Fomin, V. V. Brazhkin, V. N. Ryzhov, Transport coefficients of soft sphere fluid at high densities, *Письма в ЖЭТФ* 95 (6) (2012) 349–354.
- [19] V. Y. Rudyak, S. L. Krasnolutski, Dependence of the viscosity of nanofluids on nanoparticle size and material, *Phys. Lett. A.* 378 (26-27) (2014) 1845–1849. doi:10.1016/j.physleta.2014.04.060.
- [20] K.-S. Kim, M. H. Han, C. Kim, Z. Li, G. E. Karniadakis, E. K. Lee, Nature of intrinsic uncertainties in equilibrium molecular dynamics estimation of shear viscosity for simple and complex fluids, *The Journal of Chemical Physics* 149 (4) (2018) 044510. doi:10.1063/1.5035119.
- [21] D. M. Heyes, D. Dini, L. Costigliola, J. C. Dyre, Transport coefficients of the lennard-jones fluid close to the freezing line, *The Journal of Chemical Physics* 151 (20) (2019) 204502. arXiv:https://doi.org/10.1063/1.5128707, doi:10.1063/1.5128707. URL https://doi.org/10.1063/1.5128707
- [22] I. H. Bell, J. C. Dyre, T. S. Ingebrigtsen, Excess-entropy scaling in supercooled binary mixtures, *Nature Comms.* 11 (1) (2020) 1–12.
- [23] E. M. Kirova, G. E. Norman, V. V. Pisarev, Dynamics of changes in stress autocorrelation functions of aluminum melt during ultrafast cooling, *Computational Materials Science* 172 (2020) 109367.
- [24] A. D. Glova, I. V. Volgin, V. M. Nazarychev, S. V. Larin, S. V. Lyulin, A. A. Gurtovenko, Toward realistic computer modeling of paraffin-based composite materials: critical assessment of atomic-scale models of paraffins, *RSC Adv.* 9 (66) (2019) 38834–38847. doi:10.1039/C9RA07325F.
- [25] I. J. Prentice, X. Liu, O. A. Nerushev, S. Balakrishnan, C. R. Pulham, P. J. Camp, Experimental and simulation study of the high-pressure behavior of squalane and poly- $\alpha$ -olefins, *J. Chem. Phys.* 152 (7) (2020) 074504. doi:10.1063/1.5139723.
- [26] I. Bakulin, N. Kondratyuk, A. Lankin, G. Norman, Properties of aqueous 1,4-dioxane solution via molecular dynamics, *The Journal of Chemical Physics* 155 (15) (2021) 154501. doi:10.1063/5.0059337.
- [27] J. P. Ewen, H. A. Spikes, D. Dini, Contributions of molecular dynamics simulations to elasto-hydrodynamic lubrication, *Tribology Letters* 69 (1) (2021) 24. doi:10.1007/s11249-021-01399-w.
- [28] D. Mathas, W. Holweger, M. Wolf, C. Bohnert, V. Bakolas, J. Procelewska, L. Wang, S. Bair, C.-K. Skylaris, Evaluation of methods for viscosity simulations of lubricants at different temperatures and pressures: A case study on pa-2, *Tribology Transactions* 64 (6) (2021) 1138–1148. doi:10.1080/10402004.2021.1922790.
- [29] X. Yang, Q. Liu, X. Zhang, C. Ji, B. Cao, A molecular dynamics simulation study of the densities and viscosities of 1,2,4-trimethylbenzene and its binary mixture with n-decane, *Fluid Phase Equilib.* 562 (2022) 113566.
- [30] V. I. Deshchenya, N. D. Kondratyuk, A. V. Lankin, G. E. Norman, Molecular dynamics study of sucrose aqueous solutions: From solution structure to transport coefficients, *Journal of Molecular Liquids* 367 (2022) 120456.
- [31] V. Stegailov, E. Dlinnova, T. Ismagilov, M. Khalilov, N. Kondratyuk, D. Makagon, A. Semenov, A. Simonov, G. Smirnov, A. Timofeev, Angara interconnect makes GPU-based Desmos supercomputer an efficient tool for molecular dynamics calculations, *Int. J. High Perform. Comput. Appl.* 33 (3) (2019) 507–521. doi:10.1177/1094342019826667.
- [32] N. Kondratyuk, V. Nikolskiy, D. Pavlov, V. Stegailov, GPU-accelerated molecular dynamics: State-of-art software performance and porting from Nvidia CUDA to AMD HIP, *Int. J. High Perform. Comput. Appl.* (2021) 10943420211008288doi:10.1177/10943420211008288.
- [33] D. E. Shaw, et al., Anton 3: Twenty microseconds of molecular dynamics simulation before lunch, in: *Proceedings of the International Conference for High Performance Computing, Networking, Storage and Analysis, SC '21*, Association for Computing Machinery, New York, NY, USA, 2021.
- [34] M. Canales, L. E. González, J. A. Padró, Computer simulation study of liquid lithium at 470 and 843 k, *Phys. Rev. E* 50 (1994) 3656–3669. doi:10.1103/PhysRevE.50.3656.
- [35] N. Meyer, H. Xu, J.-F. Wax, Temperature and density dependence of the shear viscosity of liquid sodium, *Phys. Rev. B* 93 (2016) 214203.
- [36] F. Demmel, A. Tani, Stokes-Einstein relation of the liquid metal rubidium and its relationship to changes in the microscopic dynamics with increasing temperature, *Phys. Rev. E* 97 (2018) 062124. doi:10.1103/PhysRevE.97.062124.
- [37] M. Daw, M. Baskes, Embedded-atom method: Derivation and application to impurities, surfaces, and other defects in metals, *Phys. Rev. B* 29 (12) (1984) 6443.
- [38] M. Finnis, J. Sinclair, A simple empirical n-body potential for transition metals, *Philos. Mag. A* 50 (1) (1984) 45–55.
- [39] A. K. Metya, A. Hens, J. K. Singh, Molecular dynamics study of vapor-liquid equilibria and transport properties of sodium and lithium based on eam potentials, *Fluid Phase Equilib.* 313 (2012) 16–24.
- [40] E. M. Kirova, G. E. Norman, V. V. Pisarev, Simulation of the glass transition of a thin aluminum melt layer at ultrafast cooling under isobaric conditions, *JETP Letters* 2019 110:5 110 (2019) 359–363. doi:10.1134/S0021364019170089.
- [41] F. J. Cherne III, P. A. Deymier, Calculation of viscosity of liquid nickel by molecular dynamics methods, *Scripta materialia* 39 (11) (1998) 1613–1616. doi:10.1016/S1359-6462(98)00339-X.
- [42] F. J. Cherne III, M. I. Baskes, P. A. Deymier, Properties of liquid nickel: A critical comparison of eam and meam calcula-

- tions, *Phys. Rev. B* 65 (2) (2001) 024209.
- [43] M. Mendeleev, M. Kramer, C. A. Becker, M. Asta, Analysis of semi-empirical interatomic potentials appropriate for simulation of crystalline and liquid Al and Cu, *Philos. Mag.* 88 (12) (2008) 1723–1750. doi:10.1080/14786430802206482.
- [44] W. Wang, J. Han, H. Fang, J. Wang, Y. Liang, S. Shang, Y. Wang, X. Liu, L. Kecskes, S. Mathaudhu, X. Hui, Z. Liu, Anomalous structural dynamics in liquid Al<sub>80</sub>Cu<sub>20</sub>: An ab initio molecular dynamics study, *Acta Materialia* 97 (2015) 75–85. doi:10.1016/j.actamat.2015.07.001.
- [45] H. Weber, M. Schumacher, P. J v ri, Y. Tsuchiya, W. Skrotzki, R. Mazzarello, I. Kaban, Experimental and ab initio molecular dynamics study of the structure and physical properties of liquid gete, *Phys. Rev. B* 96 (2017) 054204. doi:10.1103/PhysRevB.96.054204.
- [46] Z. Rong, G. Pan, J. Lu, S. Liu, J. Ding, W. Wang, D.-J. Lee, Ab-initio molecular dynamics study on thermal property of nacl-cacl<sub>2</sub> molten salt for high-temperature heat transfer and storage, *Renewable Energy* 163 (2021) 579–588. doi:10.1016/j.renene.2020.08.152.
- [47] O. Adjaoud, G. Steinle-Neumann, S. Jahn, Transport properties of Mg<sub>2</sub>SiO<sub>4</sub> liquid at high pressure: Physical state of a magma ocean, *Earth and Planetary Science Letters* 312 (3) (2011) 463–470. doi:10.1016/j.epsl.2011.10.025.
- [48] M. Ceriotti, C. Clementi, O. Anatole von Lilienfeld, Machine learning meets chemical physics, *J. Chem. Phys.* 154 (16) (2021) 160401. doi:10.1063/5.0051418.
- [49] Y. Mishin, Machine-learning interatomic potentials for materials science, *Acta Materialia* 214 (2021) 116980. doi:10.1016/j.actamat.2021.116980.
- [50] O. A. von Lilienfeld, K. Burke, Retrospective on a decade of machine learning for chemical discovery, *Nature Communications* 11 (1) (2020) 4895. doi:10.1038/s41467-020-18556-9.
- [51] J. Behler, G. Cs nyi, Machine learning potentials for extended systems: a perspective, *Eur. Phys. J. B* 94 (7) (2021) 142. doi:10.1140/epjb/s10051-021-00156-1.
- [52] V. L. Deringer, Modelling and understanding battery materials with machine-learning-driven atomistic simulations, *Journal of Physics: Energy* 2 (4) (2020) 041003. doi:10.1088/2515-7655/abb011.
- [53] T. Mueller, A. Hernandez, C. Wang, Machine learning for interatomic potential models, *J. Chem. Phys.* 152 (5) (2020) 050902. doi:10.1063/1.5126336.
- [54] V. L. Deringer, M. A. Caro, G. Cs nyi, Machine learning interatomic potentials as emerging tools for materials science, *Advanced Materials* 31 (46) (2019) 1902765. doi:10.1002/adma.201902765.
- [55] J. Behler, Perspective: Machine learning potentials for atomistic simulations, *J. Chem. Phys.* 145 (17) (2016) 170901. doi:10.1063/1.4966192.
- [56] Y. Zuo, C. Chen, X. Li, Z. Deng, Y. Chen, J. Behler, G. Cs nyi, A. V. Shapeev, A. P. Thompson, M. A. Wood, S. P. Ong, Performance and cost assessment of machine learning interatomic potentials, *The Journal of Physical Chemistry A* 124 (4) (2020) 731–745. doi:10.1021/acs.jpca.9b08723.
- [57] T. Kostiuhenko, F. K rmmann, J. Neugebauer, A. Shapeev, Impact of lattice relaxations on phase transitions in a high-entropy alloy studied by machine-learning potentials, *npj Computational Materials* 5 (1) (2019) 1–7.
- [58] K. Nguyen-Cong, J. T. Willman, S. G. Moore, A. B. Belonoshko, R. Gayatri, E. Weinberg, M. A. Wood, A. P. Thompson, I. I. Oleynik, Billion atom molecular dynamics simulations of carbon at extreme conditions and experimental time and length scales, in: *Proceedings of the International Conference for High Performance Computing, Networking, Storage and Analysis*, 2021, pp. 1–12.
- [59] N. Orekhov, M. Logunov, Atomistic structure and anomalous heat capacity of low-density liquid carbon: Molecular dynamics study with machine learning potential, *Carbon* 192 (2022) 179–186.
- [60] N. Lopanitsyna, C. Ben Mahmoud, M. Ceriotti, Finite-temperature materials modeling from the quantum nuclei to the hot electron regime, *Phys. Rev. Materials* 5 (2021) 043802. doi:10.1103/PhysRevMaterials.5.043802.
- [61] I. Balyakin, A. Yuryev, V. Filippov, B. Gelchinski, Viscosity of liquid gallium: Neural network potential molecular dynamics and experimental study, *Computational Materials Science* 215 (2022) 111802. doi:10.1016/j.commatsci.2022.111802.
- [62] T. Feng, B. Yang, G. Lu, Investigation on the local structure and properties of molten Li<sub>2</sub>CO<sub>3</sub>-K<sub>2</sub>CO<sub>3</sub> binary salts by machine learning potentials, *Journal of Molecular Liquids* 356 (2022) 118979. doi:10.1016/j.molliq.2022.118979.
- [63] L. V. Kamaeva, R. E. Ryltsev, A. A. Suslov, N. M. Chtchelkatchev, Effect of copper concentration on the structure and properties of Al–Cu–Fe and Al–Cu–Ni melts, *Journal of Physics: Condensed Matter* 32 (22) (2020) 224003. doi:10.1088/1361-648X/ab73a6.
- [64] T. Wen, L. Zhang, H. Wang, E. Weinan, D. J. Srolovitz, Deep potentials for materials science, *Materials Futures* 1 (2) (2022) 022601. doi:10.1088/2752-5724/ac681d.
- [65] Y. Zhang, H. Wang, W. Chen, J. Zeng, L. Zhang, H. Wang, W. E, Dp-gen: A concurrent learning platform for the generation of reliable deep learning based potential energy models, *Computer Physics Communications* (2020) 107206doi:10.1016/j.cpc.2020.107206.
- [66] L. Zhang, D.-Y. Lin, H. Wang, R. Car, W. E, Active learning of uniformly accurate interatomic potentials for materials simulation, *Phys. Rev. Materials* 3 (2019) 023804. doi:10.1103/PhysRevMaterials.3.023804.
- [67] R. Ryltsev, N. Chtchelkatchev, Deep machine learning potentials for multicomponent metallic melts: Development, predictability and compositional transferability, *Journal of Molecular Liquids* 349 (2022) 118181. doi:10.1016/j.molliq.2021.118181.
- [68] H. Niu, L. Bonati, P. M. Piaggi, M. Parrinello, Ab initio phase diagram and nucleation of gallium, *Nature Communications* 11 (1) (2020) 2654. doi:10.1038/s41467-020-16372-9.
- [69] G. M. Sommers, M. F. Calegari Andrade, L. Zhang, H. Wang, R. Car, Raman spectrum and polarizability of liquid water from deep neural networks, *Phys. Chem. Chem. Phys.* 22 (2020) 10592–10602. doi:10.1039/D0CP01893G.
- [70] T. E. Gartner, L. Zhang, P. M. Piaggi, R. Car, A. Z. Panagiotopoulos, P. G. Debenedetti, Signatures of a liquid–liquid transition in an ab initio deep neural network model for water, *PNAS* 117 (42) (2020) 26040–26046. doi:10.1073/pnas.2015440117.
- [71] I. A. Balyakin, S. V. Rempel, R. E. Ryltsev, A. A. Rempel, Deep machine learning interatomic potential for liquid silica, *Phys. Rev. E* 102 (2020) 052125. doi:10.1103/PhysRevE.102.052125.
- [72] T. Wen, C.-Z. Wang, M. J. Kramer, Y. Sun, B. Ye, H. Wang, X. Liu, C. Zhang, F. Zhang, K.-M. Ho, N. Wang, Development of a deep machine learning interatomic potential for metalloid-containing pd-si compounds, *Phys. Rev. B* 100 (2019) 174101. doi:10.1103/PhysRevB.100.174101.
- [73] L. Tang, Z. J. Yang, T. Q. Wen, K. M. Ho, M. J. Kramer, C. Z. Wang, Development of interatomic potential for al–tb alloys using a deep neural network learning method, *Phys. Chem. Chem. Phys.* 22 (2020) 18467–18479. doi:10.1039/D0CP01689F.
- [74] L. Zhang, H. Wang, R. Car, W. E, Phase diagram of a deep potential water model, *Phys. Rev. Lett.* 126 (2021) 236001. doi:10.1103/PhysRevLett.126.236001.
- [75] C. M. Andolina, P. Williamson, W. A. Saidi, Optimization and validation of a deep learning cuzr atomistic potential: Robust applications for crystalline and amorphous phases with near-dft accuracy, *J. Chem. Phys.* 152 (15) (2020) 154701. doi:10.1063/5.0005347.
- [76] G. Kresse, J. Furthmuller, Efficiency of ab-initio total energy calculations for metals and semiconductors using a plane-wave basis set, *Computational Materials Science* 6 (1) (1996) 15–50. doi:10.1016/0927-0256(96)00008-0.

- [77] J. P. Perdew, J. A. Chevary, S. H. Vosko, K. A. Jackson, M. R. Pederson, D. J. Singh, C. Fiolhais, Atoms, molecules, solids, and surfaces: Applications of the generalized gradient approximation for exchange and correlation, *Phys. Rev. B* 46 (1992) 6671–6687. doi:10.1103/PhysRevB.46.6671.
- [78] J. P. Perdew, Y. Wang, Accurate and simple analytic representation of the electron-gas correlation energy, *Phys. Rev. B* 45 (1992) 13244–13249. doi:10.1103/PhysRevB.45.13244.
- [79] G. Kresse, D. Joubert, From ultrasoft pseudopotentials to the projector augmented-wave method, *Phys. Rev. B* 59 (1999) 1758–1775. doi:10.1103/PhysRevB.59.1758.
- [80] F. Müller-Plathe, Reversing the perturbation in nonequilibrium molecular dynamics: An easy way to calculate the shear viscosity of fluids, *Phys. Rev. E* 59 (1999) 4894–4898. doi:10.1103/PhysRevE.59.4894.
- [81] S. Plimpton, Fast parallel algorithms for short-range molecular dynamics, *J. Comput. Phys.* 117 (1) (1995) 1–19.
- [82] N. D. Kondratyuk, V. V. Pisarev, Calculation of viscosities of branched alkanes from 0.1 to 1000 mpa by molecular dynamics methods using compass force field, *Fluid Phase Equilibria* 498 (2019) 151–159. doi:10.1016/j.fluid.2019.06.023.
- [83] N. Kondratyuk, Contributions of force field interaction forms to Green-Kubo viscosity integral in n-alkane case, *J. Chem. Phys.* 151 (2019) 074502. doi:10.1063/1.5103265.
- [84] Y. Zhang, A. Otani, E. J. Maginn, Reliable Viscosity Calculation from Equilibrium Molecular Dynamics Simulations: A Time Decomposition Method, *J. Chem. Theory Comput.* 11 (8) (2015) 3537–3546. doi:10.1021/acs.jctc.5b00351.
- [85] S. Nosé, A molecular dynamics method for simulations in the canonical ensemble, *Mol. Phys.* 52 (2) (1984) 255–268. doi:10.1080/00268978400101201.
- [86] W. G. Hoover, Canonical dynamics: Equilibrium phase-space distributions, *Phys. Rev. A* 31 (1985) 1695–1697. doi:10.1103/PhysRevA.31.1695.
- [87] W. Shinoda, M. Shiga, M. Mikami, Rapid estimation of elastic constants by molecular dynamics simulation under constant stress, *Phys. Rev. B* 69 (2004) 134103. doi:10.1103/PhysRevB.69.134103.
- [88] X. J. Han, M. Chen, Y. J. Lü, Transport properties of undercooled liquid copper: A molecular dynamics study, *International Journal of Thermophysics* 29 (4) (2008) 1408–1421. doi:10.1007/s10765-008-0489-7.
- [89] W. Götze, *Complex Dynamics of Glass-Forming Liquids: A Mode-Coupling Theory*, Vol. 9780199235, Oxford University Press, 2009. doi:10.1093/acprof:oso/9780199235346.001.0001.
- [90] N.-T. Van-Oanh, C. Houriez, B. Rousseau, Viscosity of the 1-ethyl-3-methylimidazolium bis(trifluoromethylsulfonyl)imide ionic liquid from equilibrium and nonequilibrium molecular dynamics, *Phys. Chem. Chem. Phys.* 12 (2010) 930–936. doi:10.1039/B918191A.
- [91] R. Safinejad, N. Mehdipour, H. Eslami, Atomistic reverse nonequilibrium molecular dynamics simulation of the viscosity of ionic liquid 1-n-butyl 3-methylimidazolium bis(trifluoromethylsulfonyl)imide [bmim][Tf2N], *Phys. Chem. Chem. Phys.* 20 (2018) 21544–21551. doi:10.1039/C8CP02393J.
- [92] M. Tan, B. Xiufang, X. Xianying, Z. Yanning, G. Jing, S. Baoan, Correlation between viscosity of molten Cu–Sn alloys and phase diagram, *Physica B: Condensed Matter* 387 (1) (2007) 1–5. doi:10.1016/j.physb.2005.10.140.
- [93] A. L. Belyukov, V. I. Ladyanov, Viscosity of Fe-P melts in the range 5–25 at % P, *Russian Metallurgy (Metally)* 2010 (2) (2010) 128–132. doi:10.1134/S0036029510020102.
- [94] V. Ladyanov, A. Belyukov, S. Menshikova, A. Korepanov, Viscosity of Al–Ni and Al–Co melts in the Al-rich area, *Physics and Chemistry of Liquids* 52 (1) (2014) 46–54. doi:10.1080/00319104.2013.793599.
- [95] S. Mudry, V. Vus, A. Yakymovych, Influence of ni additions on the viscosity of liquid al2cu, *High Temperature Materials and Processes* 36 (7) (2017) 711–715. doi:doi:10.1515/htmp-2015-0190.
- [96] R. P. Chhabra, D. K. Sheth, Viscosity of molten metals and its temperature dependence, *International Journal of Materials Research* 81 (4) (1990) 264–271. doi:10.1515/ijmr-1990-810408.
- [97] N. Y. Konstantinova, P. S. Popel’, D. A. Yagodin, The kinematic viscosity of liquid copper-aluminum alloys, *High Temperature* 47 (3) (2009) 336–341. doi:10.1134/S0018151X09030067.
- [98] N. V. Olyanina, A. L. Belyukov, V. I. Ladyanov, Viscosity of Co-B melts, *Russian Metallurgy (Metally)* 2016 (2) (2016) 150–155. doi:10.1134/S0036029516020105.
- [99] R. F. Brooks, A. T. Dinsdale, P. N. Quedstedt, The measurement of viscosity of alloys — A review of methods, data and models, *Measurement Science and Technology* 16 (2) (2005) 354–362. doi:10.1088/0957-0233/16/2/005.
- [100] J. Cheng, J. Gröbner, N. Hort, K. U. Kainer, R. Schmid-Fetzer, Measurement and calculation of the viscosity of metals—a review of the current status and developing trends, *Measurement Science and Technology* 25 (6) (2014) 062001. doi:10.1088/0957-0233/25/6/062001.
- [101] A. T. Dinsdale, P. N. Quedstedt, The viscosity of aluminium and its alloys — A review of data and models, *Journal of Materials Science* 39 (24) (2004) 7221–7228. doi:10.1023/B:JMSC.0000048735.50256.96.
- [102] W. Chen, L. Zhang, Y. Du, B. Huang, Viscosity and diffusivity in melts: from unary to multicomponent systems, *Philosophical Magazine* 94 (14) (2014) 1552–1577. doi:10.1080/14786435.2014.890755.
- [103] A. L. Belyukov, V. I. Ladyanov, An automated setup for determining the kinematic viscosity of metal melts, *Instruments and Experimental Techniques* 51 (2) (2008) 304–310. doi:10.1134/S0020441208020279.
- [104] P. S. Kostenetskiy, R. A. Chulkevich, V. I. Kozyrev, HPC resources of the higher school of economics, *Journal of Physics: Conference Series* 1740 (2021) 012050. doi:10.1088/1742-6596/1740/1/012050.